Research Article Vol. 16, No. 2 / 1 Feb 2026 / Optical Materials Express 294
Optical Materials EXPRESS

Revisiting energy transfer in Tm-doped aluminosilicate glass fiber II: variation of the Tm-doping concentration

MARTIN P. BUCKTHORPE,[1,*] RICHARD ŠVEJKAR,[2] W. ANDREW CLARKSON,[2] AND STUART D. JACKSON[1]

[1]MQ Photonics, School of Engineering, Macquarie University, North Ryde 2109, Australia
[2]Optoelectronics Research Centre, University of Southampton, University Rd., Southampton SO17 1BJ, United Kingdom
[*]martin.buckthorpe@mq.edu.au

Abstract: We extend our model that aims to quantify energy transfer in the Tm^{3+}-doped aluminosilicate glass system to the analysis of a range of Tm^{3+} concentrations spanning more than an order of magnitude. We introduce energy migration to the model and find that its rate parameter has a linear dependence on the Tm^{3+} concentration, in contrast to energy transfer upconversion and in particular cross relaxation which vary nonlinearly. When we compare our results of the cross relaxation rate with those reported in the literature for other glass and crystal hosts, we find that the functional dependence with the Tm^{3+} concentration is markedly different, suggesting that the host composition of aluminosilicate glass presents unique energy transfer properties for Tm^{3+}-doped fibers.

1. Introduction

Quantifying the energy transfer parameters in rare earth doped gain media allows a better understanding of the performance of the laser process and provides the groundwork criterion for optimization. In rare earth doped glass, energy transfer is complicated by the degree of heterogeneity of the local rare earth environment and critically, by the degree of uniformity of the doping throughout the matrix. Thus, unlike crystalline systems whereby rare earth ions can substitute for atoms of the native host providing a relatively homogeneous doped system, rare earth doped glasses are more challenging when quantification of energy transfer is needed. Accurate understanding of the doping level, host composition and the fabrication conditions are considered the essential starting points for detailed energy transfer analysis of rare earth doped glass.

An excellent example illustrating the complications arising from the glassy nature of the host is the Tm^{3+}-doped aluminosilicate glass system. Typically studies have concentrated on improving the slope efficiency, a parameter which is proportional to the level of cross relaxation (CR) [1,2] but, because of the issues outlined above, we observe a significant variation in the measured slope efficiency and threshold across these studies [3]. Not only is the fiber and hence laser prone to intrinsic host issues, contamination from OH and other impurities also impacts lasing. The associated energy transfer parameters, in particular the CR rate extracted from the reported time domain fluorescence measurements mirrors this variance [4–7]. Complications also arise from the sheer number of energy transfer processes that are possible for the Tm^{3+} ion system, making accurate quantification of the energy transfer analysis difficult. As a result, most studies have concentrated on pushing the power [8] and efficiency with recent studies reaching close to theoretical limits [9,10].

In a companion paper [11] we introduced a model for Tm^{3+}-doped aluminosilicate glass that provides a basis for quantification of energy transfer. The starting point for the model was

#581022 https://doi.org/10.1364/OME.581022
Journal © 2026 Received 7 Oct 2025; revised 3 Dec 2025; accepted 3 Dec 2025; published 15 Jan 2026

Optical Materials EXPRESS

evaluation of the intrinsic decay into two components each relating to the two local environments associated with the Tm^{3+} ions when doped into aluminosilicate glass. This approach to the calibration of the intrinsic decay relied on the validity of data taken from the literature [12,13] combined with the primary assumptions that no clustering or energy transfer is present for Tm^{3+} doping levels <100 ppm molar i.e., for these concentrations intrinsic decay is the sole deactivation process. The second component to the model was segmentation of the measured time domain fluorescence into regions in which a set of energy transfer processes dominate so that these parameters can be determined using simple curve fitting. For example, CR was assumed to be the sole energy transfer process in the initial part of the fluorescence decay for the $^3H_4$ energy level. The restriction to a single energy transfer process was evaluated statistically providing the optimum time segment for quantification. This process was also applied to the estimation of energy transfer upconversion (ETU) for the $^3F_4$ level. The model was restricted to the two metastable energy levels that are considered relevant to the analysis of Tm^{3+}-doped aluminosilicate glass. The weakness of the model was that it was introduced using a single fiber meaning the proper evaluation and applicability of the model was limited.

In this follow up report, we extend this model to the analysis of a range of Tm^{3+}-doped aluminosilicate glass fibers in which the Tm^{3+} concentration is varied by more than one order of magnitude. These fibers were also investigated in another recent publication [14], which determined the variation of quantum efficiency and background propagation loss with Tm^{3+}-doping concentration. The fibers, fabricated at the Optoelectronics Research Centre (ORC), University of Southampton, were initially analyzed for accurate Al_2O_3 composition as this is the primary starting point for the analysis. Importantly, we introduce energy migration to the model and estimate its functional dependence on Tm^{3+} concentration. We used the fluorescence decay segmentation and curve fitting approach to quantify energy transfer as a function of Tm^{3+} concentration allowing easy extraction of the fundamental parameters for energy transfer. We compared our values for CR with the reported values from the literature and show that the functional dependence on the Tm^{3+} concentration for aluminosilicate glass is distinctly different to most other hosts.

2. Theory

Figure 1 shows the energy level diagram of Tm^{3+}-doped silica. Optical pumping at 0.79 μm is typically employed for laser devices due to the strong optical absorption into the $^3H_4$ level and the availability of high-power fiber-coupled AlGaAs diode lasers emitting at this wavelength. The well-known CR and ETU processes are also shown in Fig. 1. To maximize the efficiency, the design and composition of the laser glass aims to maximize the CR process which usually means the incorporation of a higher Tm^{3+}-doping concentration. The design of the laser glass also aims to reduce the rate of ETU processes, which depopulates the pump level ($^3H_4$) and the upper laser level ($^3F_4$) [2]. The rate of CR and ETU are typically increased by the onset of Tm^{3+} ion clustering, which effectively increases the local Tm^{3+} concentration meaning energy transfer is enhanced, sometimes considerably.

A novel method of determining the mean intrinsic lifetime of a Tm^{3+} ion in an aluminosilicate environment, τ_{intr}, was proposed in the previous study [11]. This approach expressed the intrinsic decay as the sum of two exponential functions, and as is shown in Eq. (1).

$$\tau_{intr} = \frac{1}{I_0}\int_0^\infty I_{intr}(t)dt = \int_0^\infty \left[A\exp\left(\frac{-t}{\tau_s}\right) + (1-A)\exp\left(\frac{-t}{\tau_{as}}\right)\right]dt \tag{1}$$

Here, $I_{intr}(t)$ is the intensity of fluorescence from a single excited ion in the host environment due to intrinsic decay at time t. The partitioning parameter A is introduced to describe the proportion of ions occupying a silicate-rich environment, with a higher local phonon energy and hence a greater rate of NR decay. The assumption is made that the remaining ions occupy an

Optical Materials EXPRESS

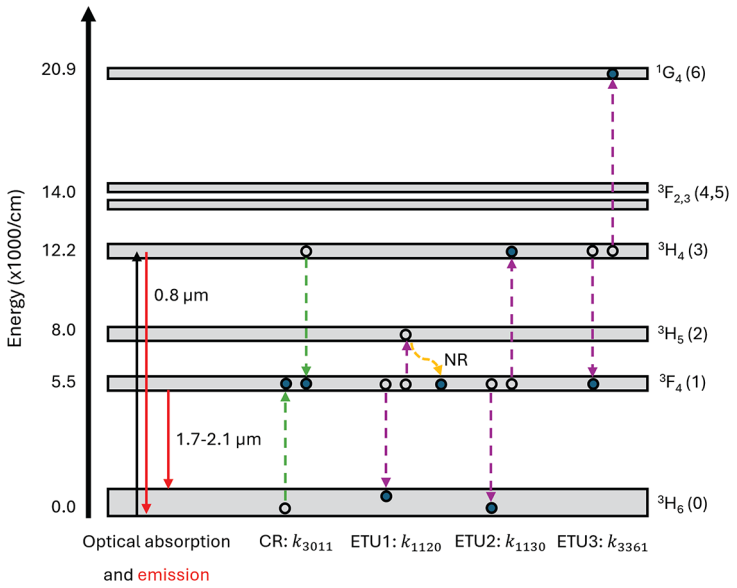

Fig. 1. A typical energy level diagram of a Tm^{3+}-doped silica fiber. The key optical absorption, optical emission, cross-relaxation (CR) [1], and energy transfer upconversion (ETU) [2] processes are highlighted.

aluminum-rich environment, with a lower local phonon energy and a reduced rate of NR decay. The values of τ_s, τ_{as} and A can be found via a review of the literature as discussed previously [11]. I_0 is the initial intensity at t=0, which is equal to 1 when the decays are normalized.

The intensity of optical fluorescence of a given energy level of a rare earth doped laser medium, $I(t)$, is given by the Burshtein expression [15], as shown in Eq. (2).

$$I(t) = I_0 \exp\left(-\frac{t}{\tau_m} - \gamma_{ET}\sqrt{t}\right) \tag{2}$$

Here, τ_m represents the sum of decay processes that decrease in strength linearly as the population of the excited state decreases over time. The radiative decay, nonradiative (NR) decay and energy migration (EM) processes are grouped into the term τ_m, as shown in Eq. (3).

$$\frac{1}{\tau_m} = \frac{1}{\tau_R} + W_{NR} + \omega_{EM} = \frac{1}{\tau_{intr}} + \omega_{EM} \tag{3}$$

Here, τ_R is the radiative lifetime of the decaying level and W_{NR} is the rate of NR decay. The term ω_{EM} describes the rate at which the excited state 'migrates' or 'diffuses' through the medium. This process involves the transfer of the excitation from an excited Tm^{3+} ion to one of its neighbors, resulting in the donor ion relaxing to the ground state while the acceptor ion is excited to the same excited state that the donor initially occupied [15]. Therefore, this is a process by which energy is considered to be preserved. Energy migration can have a significant role in systems such as Tm^{3+}-doped aluminosilicate glass where there is considerable resonance between the absorption and emission bands of energy levels, which is the result of inhomogeneous broadening of the transition spectra.

As shown by the Inokuti-Hirayama model of dipole-dipole energy transfer [16], the time domain characteristic of energy transfer processes (such as CR and ETU) in the fluorescence decay varies with $\sqrt{t}$. When considering only dipole-dipole interactions, the energy transfer

Optical Materials EXPRESS

parameter, γ_{ET}, is described by Eq. (4).

$$\gamma_{ET} = \sqrt{\pi}\frac{C}{C_0}\frac{1}{\sqrt{\tau_{intr}}} = \sqrt{\pi}\left(\frac{R_0}{R_{Tm}}\right)^3\frac{1}{\sqrt{\tau_{intr}}} \tag{4}$$

Here, C is the average concentration and R_{Tm} is the average separation distance of Tm^{3+} ions present in the medium. The terms C_0 and R_0 are the critical concentration and critical ion separation distance, respectively, and originate from Foster energy transfer theory [16,17]. For an isolated donor-acceptor pair, the term R_0 represents the separation distance at which the rate of energy transfer equals the rate of spontaneous deactivation of the donor. When applied globally, this is simply converted to an effective critical concentration via the expression $C_0 = \frac{3}{4\pi R_0^3}$ [16,17]. The critical concentration is defined with respect to Tm^{3+} acceptor ions occupying a spherical volume around a Tm^{3+} donor ion. Therefore, the average concentration of the sample under test, C, has been defined in the same way.

By applying the Burshtein model to a Tm^{3+}-doped aluminosilicate system, whilst including expression of the intrinsic host-related decay, the mean luminescence lifetime, τ, can be given by Eq. (5).

$$\tau = \frac{1}{I_0}\int_0^\infty I(t)dt = \int_0^\infty \left[A\exp\left(\frac{-t}{\tau_s}\right) + (1-A)\exp\left(\frac{-t}{\tau_{as}}\right)\right]\exp\left(-\omega_{EM}t - \gamma_{ET}\sqrt{t}\right)dt \tag{5}$$

The assumption is made that there is a single dominating energy transfer process leading to an increase in the rate of fluorescence decay of a given Tm^{3+} energy level. Therefore, the rate of energy transfer, W_{ET}, is given by Eq. (6).

$$W_{ET} = \frac{1}{\tau} - \frac{1}{\tau_m} \tag{6}$$

The energy transfer coefficient of the transfer process, k_{iiff}, is given by Eq. (7).

$$k_{iiff} = \frac{W_{ET}}{N_{Tot}} \tag{7}$$

Here, i and f represent the initial and final energy levels of the energy transfer process, respectively. As shown previously [11], application of Eq. (7) to determine the CR coefficient is valid in the limit of low incident pump power to the fiber. This is because the impact of other competing power-dependent processes (such as ETU3) is minimized. Determining the coefficient of the ETU1 and ETU2 processes de-populating the $^3F_4$ level is valid in the limit of high incident pump power to the fiber, where the pump absorption is saturated. In this limit the assumption is made that all ions occupy the metastable $^3F_4$ level and the populations of the other energy levels are negligible. These rate coefficients can be used to build up the well-known rate equations for further modeling of the laser system.

3. Fiber details

To determine the energy transfer parameters as a function of Tm^{3+}-doping concentration, a controlled range of Tm^{3+}-doped aluminosilicate fibers were used in this study. These fibers were fabricated at the Optoelectronics Research Center (ORC), University of Southampton via the conventional modified chemical vapour deposition (MCVD) and solution doping processes [14]. During fabrication, the inner layer of Heraeus F300 silica tubes were deposited with silica cladding layers. Next, the silica soot that formed the cores was deposited under a constant temperature of 1400 +/- 40 °C to control the porous nature. A solution containing $TmCl_3{\cdot}6H_2O$ (99.9999 %) and $AlCl_3{\cdot}6H_2O$ (99.999 %) was used for the solution doping process. The Al

Optical Materials EXPRESS

concentration of the solution was maintained at a constant level, while the Tm concentration was systematically varied. The soot layer of each sample was dried with Cl_2 gas to ensure low levels of OH contamination. The samples were then oxidized and sintered, before finally collapsed to form the fiber preforms. These were drawn into fibers with average cladding diameters of 125 μm and a high-index polymer coating applied. The average core diameter was 12.7 +/- 0.5 μm across the fibers. The composition of the fibers examined in this study is summarized in Table 1.

Table 1. A summary of the composition of each fiber examined in this study [14] and the 0.2 wt.% fiber from [11].

Fiber ID	Tm^{3+}-doping (at. wt.%)	Tm_2O_3-doping (mol.%)	Al_2O_3-doping (mol.%)	*A* parameter (from Eq. (2) of [11])	OH contamination level (ppm)
0 (from [11])	0.2±0.1	0.02±0.01	2.9±0.1	0.50±0.01	Assumed <5
1	0.4±0.1	0.03±0.01	1.9±0.1	0.65±0.02	3.4±0.1
2	1.1±0.1	0.09±0.01	3.2±0.1	0.47±0.01	4.9±0.1
3	2.3±0.1	0.19±0.01	4.4±0.1	0.34±0.01	2.7±0.1
4	3.1±0.1	0.25±0.01	3.2±0.1	0.47±0.01	3.3±0.1
5	3.9±0.1	0.32±0.01	4.0±0.1	0.38±0.01	4.0±0.1
6	4.8±0.1	0.39±0.01	3.9±0.1	0.38±0.01	2.6±0.1

The Tm^{3+}-doping concentrations were determined via measurement of the core absorption at 790 nm and the Al_2O_3-doping concentrations were determined via energy dispersive x-ray (EDX) measurements across the cores of the fiber preforms [14]. Some variation in the Al_2O_3-doping concentrations was measured across the samples. This is expected to lead to variation in the intrinsic decay rates of each fiber, which was accounted for in this analysis via application of Eq. (1). The OH contamination levels were determined from transmission measurements at the typical OH absorption peaks (1375 nm and 2200 nm) [14,18]. The assumption is made that the levels of OH contamination in these fibers are sufficiently low to not significantly impact the shape of the $^3F_4$ fluorescence decays.

4. Results

4.1. Fluorescence decay measurements of the $^3H_4$ level

Using the same experimental setup as described previously [11], fluorescence decay measurements of the $^3H_4$ level were recorded by collecting 0.8 μm side light from the fibers at the pump input splice. Analysis of the CR rate was completed by applying least-means-squared curve-fitting to the measured fluorescence decays at a launched pump power of 78 mW. This was the second-lowest pump power utilized, and was chosen for the fit to provide a sufficient signal to noise ratio, whilst minimizing the impact of power-dependent processes such as ETU3. The only exception was the 2.3 wt.% fiber, whereby low detected signal levels resulting from experimental misalignment required a pump power of 130 mW to be utilized for analysis of the $^3H_4$ fluorescence decay. Figure 2 shows an example of the fit of the energy transfer model to the $^3H_4$ raw decay data of the 4.8 wt.% fiber at a pump power of 78 mW.

Our previous study analyzed the value of γ_{CR} as a function of decay time segment, and concluded that these fits are optimized over 25 μs [11]. An important distinction to address here is that this study includes the influence of energy migration as an additional parameter to the curve fitting, compared to our previous model. This gives rise to two important results: Firstly, the curve fitting produces a closer match to the experimental decays when energy migration is included, as demonstrated by the close fit of the $^3H_4$ fluorescence decay of the 4.8 wt.% fiber at 78 mW pump power. Here, R^2 = 0.974 when using γ_{CR} as a fitting parameter, compared to

Optical Materials EXPRESS

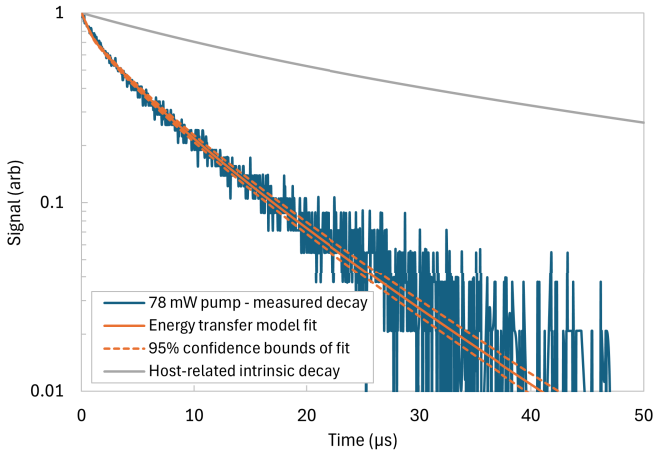

Fig. 2. Fit of the energy transfer model to the $^3H_4$ raw decay data of the 4.8 wt% with a pump power of 78 mW. Here, $\gamma_{CR} = 0.2076\ \mu s^{-1/2}$ and $\omega_{EM}^{3H4} = 0.052\ \mu s^{-1}$, giving a close fit with $R^2 = 0.99$.

$R^2 = 0.99$ using both γ_{CR} and ω_{EM}^{3H4} as fitting parameters. The second difference observed is the trend in γ_{CR} from 25-50 μs. In this study, both γ_{CR} and ω_{EM}^{3H4} appear to reach stable values over time windows longer than 25 μs. In our previous study, γ_{CR} continued to increase from 25-50 μs. It is believed that this may have been due to ETU3 having an increased impact on the shape of the decay over longer timescales. However, this may have also been caused by fitting an incomplete energy transfer model within this time segment that did not include the effect of energy migration. As shown in Fig. 3 (example shown is the 4.8 wt.% fiber), the values of γ_{CR} and ω_{EM}^{3H4} obtained during this study do not change significantly after 25 μs. Instead, each parameter appears to reach a consistent value. Thus, the values of γ_{CR} and ω_{EM}^{3H4} were taken over a time segment of 50 μs to ensure sampling of the largest quantity of measured data to maximize accuracy. The error bars shown here represent 95% confidence bounds of the curve fitting. Therefore, the integrals in Eq. (1) and Eq. (5) were also evaluated up to 50 μs.

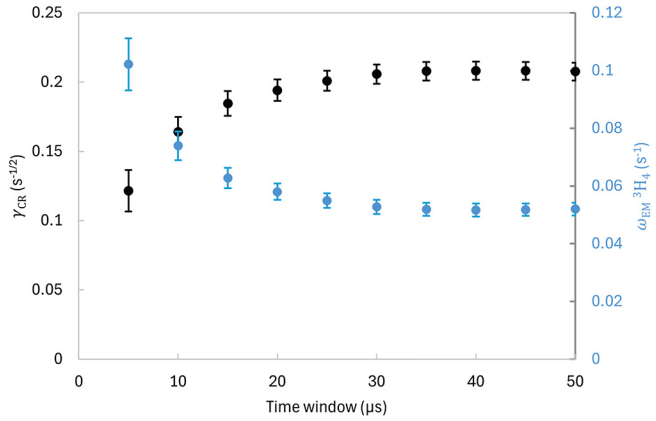

Fig. 3. The values of γ_{CR} and ω_{EM}^{3H4} as a function of the total time segment of the fluorescence decay sampled. The values in this example were extracted from the $^3H_4$ fluorescence decay of the 4.8 wt.% fiber at a pump power of 78 mW.

Optical Materials EXPRESS

Figure 4 shows the results of CR rate, W_{CR}, and its differential as a function of Tm^{3+}-doping concentration. The curve fit to the CR rate follows a power law of a_{CR} x ${N_{Tm}}^{b_{CR}}$, where a_{CR} = 25,000 +/- 5,000 and b_{CR} = 0.34 +/- 0.13. It is expected that the rate of CR will increase with the average Tm^{3+}-doping concentration, due to the reduction in the average ion separation distance. However, the key finding of these measurements is the shape of CR rate with concentration. The increase in CR rate appears to be initially quite rapid for very low concentrations. This contrasts with most other reported measurements, discussed in detail later. These results suggest that the CR process plays a critical role even for Tm^{3+}-doping concentrations lower than 0.4 wt.%. This is also supported by the findings in our companion paper [11], where high levels of energy transfer were measured at the low Tm^{3+}-doping concentration of 0.2 wt.%, which is also shown in Fig. 4. Note that we have corrected this value for γ_{CR} compared to our previous paper [11] now that EM has been included. Nevertheless, the 0.2 wt.% fiber displays anomalously high CR rates relative to the current set of fibers. It is clear that despite the sufficient levels of Al_2O_3 in this fiber, some agglomeration of Tm^{3+}-doping may be occurring leading to enhanced energy transfer.

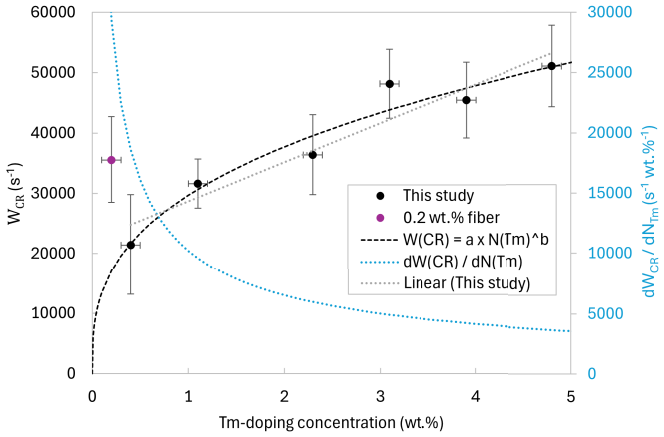

Fig. 4. The calculated values of W_{CR} as a function of Tm^{3+}-doping concentration for the fibers in this study and the 0.2 wt.% fiber from [11]. Also shown is the derivative of the W_{CR} trace to highlight the rate of change in W_{CR} with Tm^{3+}-doping concentration.

The rapid increase in the values for W_{CR} also leads to significantly higher values for the calculated CR coefficient k_{3011} (see Eq. (7)) at lower Tm^{3+}-doping concentrations. The reason for this rapid increase is unclear, however it may still be the result of some agglomeration effects occurring at low average Tm^{3+}-doping concentrations for this set of fibers. Note we are avoiding the use of the word clustering here in order to stress that agglomeration may not be so detrimental as is normally associated with clustering. Agglomeration may be a feature of the conventional silicate fiber fabrication methods, whereby the uniformity of doping is highly dependent on the properties of the porous silicate soot which is deposited during MCVD and filled with doping elements during the solution doping phase. Note that we have included in Fig. 4 the differential of the curve fit to W_{CR} with respect to the Tm^{3+}-doping concentration in order to highlight the rapid change in W_{CR} at lower concentrations. The rate of increase in the value for W_{CR} with increasing Tm^{3+}-doping concentration becomes more gradual and appears to linearize at higher levels of doping, indicating that the effects from agglomeration are lower; the linearization of W_{CR} with concentration is seen in the differential of W_{CR} which is asymptotic to a value above zero as the concentration is increased. Above a Tm^{3+}-doping concentration of 3 wt.%, the benefits of further improving the CR rate appear to be diminishing. This agrees with the findings of a separate study into the quantum efficiency and background propagation loss of the same Tm^{3+}-doped fibers as studied here [14]. The referenced study found that increasing the Tm^{3+}-doping concentration

Optical Materials EXPRESS

above approximately 3 wt.% provides diminishing returns for increasing the quantum efficiency. It should be noted that other studies of laser efficiency as a function of Tm^{3+}-doping concentration have also found optimum performance around at 3-4 wt.% [19].

Figure 5 shows the energy migration rate of the $^3H_4$ energy level as a function of the Tm^{3+}-doping concentration. As with the analysis of the CR rate, these values were obtained from the curve fitting of the measured fluorescence decays at a launched pump power of 78 mW, over a 50 μs time segment. The values of ω_{EM}^{3H4} are comparable to the values of W_{CR}. We stress that inclusion of energy migration is an important parameter in the analysis because it has a non-negligible impact on the value of τ_m^{3H4}, and hence W_{CR}. It is interesting to note that the rapid change in W_{CR} with concentration is not seen with ω_{EM}^{3H4} and a simple linear increase with concentration is observed. This is expected given the steady decrease in the Tm^{3+} ion separation as the concentration is increased, however it is not clear why EM is not affected by agglomeration of the Tm^{3+} ions as is postulated for CR given that both processes involve a ground state ion. It is clear that more work is required to understand the interplay between CR and EM for the Tm^{3+}-doped aluminosilicate glass system.

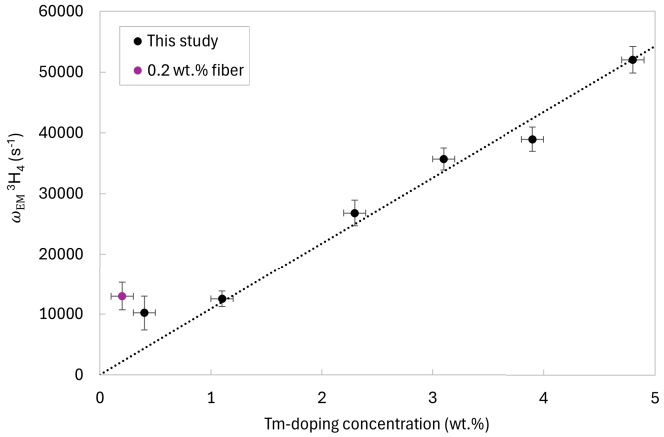

Fig. 5. Energy migration rate parameter of the $^3H_4$ energy level, ω_{EM}^{3H4}, as a function of Tm^{3+}-doping concentration for the fibers in this study and the 0.2 wt.% fiber from [11]. These values were obtained at a launched pump power of 78 mW.

A complete summary of the results obtained from analysis of the $^3H_4$ fluorescence decays can be found in Table 2.

4.2. *Fluorescence decay measurements from $^3F_4$ level*

A similar analysis was applied to measurements of the $^3F_4$ fluorescence decay, to assess the effect of the ETU1 and ETU2 processes on de-populating this level. Here, the fluorescence is emitted at a wavelength of 1.8 μm. Figure 6 shows an example of the fit of the energy transfer model to the $^3F_4$ raw decay data of the 4.8 wt.% fiber, recorded at 330 mW launched pump power.

Figure 7 shows the relationship between the combined rate of the ETU1 and ETU2 processes, W_{ETU1+2}, and Tm^{3+}-doping concentration. As expected, W_{ETU1+2} increases with Tm^{3+}-doping concentration. However, the shape of the trend is considerably different to the trend observed for CR (see Fig. 4). Here, the ETU trend follows a simple power law of a_{ETU1+2} x ${N_{Tm}}^{b_{ETU1+2}}$ where a_{ETU1+2} = 620 +/- 180 and b_{ETU1+2} = 1.33 +/- 0.21. Overall, the combined rates of ETU1 and ETU2 are approximately an order of magnitude weaker than the rate of CR. This is likely to be for two reasons; because ETU1 is a process that has lower resonance, and because ETU2 is an endothermic process that requires an energy contribution from phonons, whereas

Optical Materials EXPRESS

Table 2. A summary of the results obtained by analysis of the $^3H_4$ fluorescence decays of the fibers in this study and the 0.2 wt.% fiber from [11]. The results of the 0.2 wt.% fiber from [11] have been adjusted to include the contribution from EM. These values (including τ_{intr}^{3H4}) were obtained from analysis of a 50 μs decay window at a launched pump power of 78 mW (apart from the 2.3 wt.% fiber which was analyzed at 130 mW).

Fiber ID	τ_{intr}^{3H4} (μs)	τ^{3H4} (μs)	W_{CR} (10^3 s^{-1})	k_{3011} (10^{-22} m^3s^{-1})	ω_{EM}^{3H4} (10^3 s^{-1})
0 (from [11])	23.9±0.3	11.1±0.6	35.5±7.2	12-55	12.9±2.3
1	21.0±0.3	12.6±0.9	21.4±8.3	3.4-12.7	10.2±2.8
2	24.5±0.2	11.8±0.4	31.6±4.1	2.9±0.9	12.5±1.3
3	27.2±0.2	10.0±0.5	36.4±6.6	2.0±0.5	26.8±2.1
4	24.6±0.2	8.0±0.3	48.2±5.7	2.0±0.3	35.7±1.8
5	26.3±0.2	8.2±0.3	45.5±6.3	1.5±0.3	38.9±2.0
6	26.2±0.2	7.1±0.2	51.1±6.8	1.4±0.2	52.0±2.2

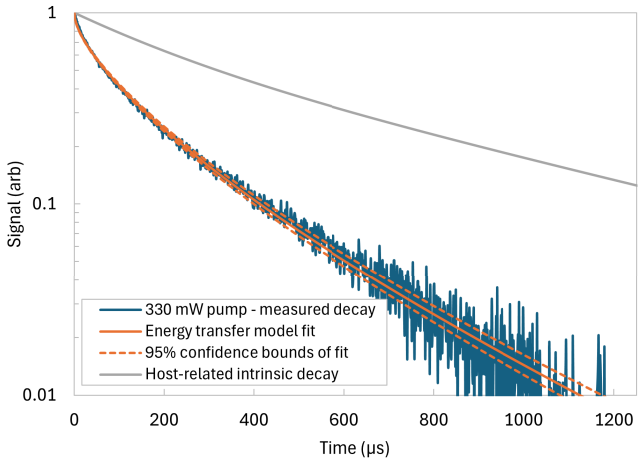

Fig. 6. Fit of the energy transfer model to the $^3F_4$ raw decay data of the 4.8 wt% fiber, recorded at 330 mW launched pump power. Here, $\gamma_{ETU1+2} = 0.0568\ \mu s^{-1/2}$ and $\omega_{EM}^{3F4} = 0.0007\ \mu s^{-1}$, giving a close fit with $R^2 = 0.997$.

CR is an exothermic process and thus should have a comparatively higher rate parameter [2]. Included in Fig. 7 is the differential of the curve fit to W_{ETU1+2} with respect to the Tm^{3+}-doping concentration, calculated to highlight the change in W_{ETU1+2} with concentration. Future studies should concentrate on analyzing the CR, ETU and EM rates for a range of fibers with Tm^{3+} concentrations <1 wt.% because it is in this region that our results are lacking definitive characterization. Nonetheless, it is clear that the differential of the curve fit for W_{ETU1+2} is reaching an asymptote as the concentration is increased. Note that the value for the W_{ETU1+2} for the 0.2 wt.% fiber is also included in Fig. 7 whereby the effects from agglomeration of the Tm^{3+} ion doping distribution may be present, although we stress we cannot say this conclusively.

Figure 8 shows the values of γ_{ETU1+2} and ω_{EM}^{3F4} as a function of launched pump power, for the 4.8 wt.% fiber. It is widely known that ETU processes get stronger as the excitation power increases due to the increase in the population densities of the excited states. Conversely, the rate of energy migration appears to decrease with pump power. This seems logical, since energy migration involves energy transfer to a local ion occupying the ground state which are becoming fewer as we reach pump saturation. A simple saturating function was applied to the γ_{ETU1+2}

Optical Materials EXPRESS

results to determine its value in the limit of high power. This function had the form as shown in Eq. (8).

$$\gamma_{ETU1+2} = \gamma_{ETU1+2}^{high}\left(1 - \frac{1}{1+\left(\frac{P}{P_{sat}}\right)^{d}}\right) \tag{8}$$

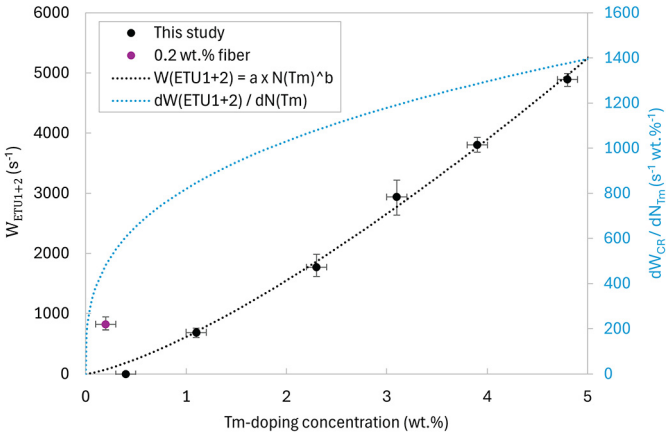

Fig. 7. The calculated values of W_{ETU1+2} as a function of Tm^{3+}-doping concentration for the fibers in this study and the 0.2 wt.% fiber from [11]. Also shown is the derivative of the W_{ETU1+2} trace to highlight the rate of change in W_{ETU1+2} with Tm^{3+}-doping concentration.

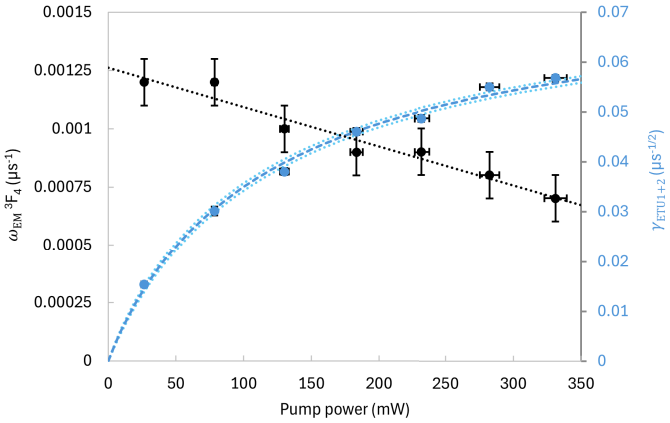

Fig. 8. The values of the γ_{ETU1+2} and ω_{EM}^{3F4} parameters for the 4.8 wt.% fiber, obtained from the measured $^3F_4$ fluorescence decays, as a function of launched pump power.

Here, P is launched pump power and γ_{ETU1+2}^{high}, P_{sat} and d were variables which were determined for each fiber via least-means-squared curve fitting. In the limit of high pump power, the value of γ_{ETU1+2} becomes γ_{ETU1+2}^{high} and the value of ω_{EM}^{3F4} was taken as 0, since the assumption here is that the majority of ions occupy the metastable $^3F_4$ level, and the population of the $^3H_6$ ground state is negligible. This appears to be a valid assumption considering the trend of ω_{EM}^{3F4} decreasing as the pump power is increased, which is shown in Fig. 8. Also shown in Fig. 8 is an example of the application of Eq. (8) to the values of γ_{ETU1+2} as a function of pump power, P, for the 4.8 wt.% fiber.

Optical Materials EXPRESS

Using simple linear fits to the results of ω_{EM}^{3F4} as a function of launched pump power, the values of ω_{EM}^{3F4} at a hypothetical pump power of 0 mW were determined. Figure 9 shows how these results vary with Tm^{3+}-doping concentration. Similar to the energy migration trends for the $^3H_4$ level, the energy migration of the $^3F_4$ level increases approximately linearly with Tm^{3+}-doping concentration. Interestingly, the energy migration rate of the $^3H_4$ level is much greater than the $^3F_4$ level.

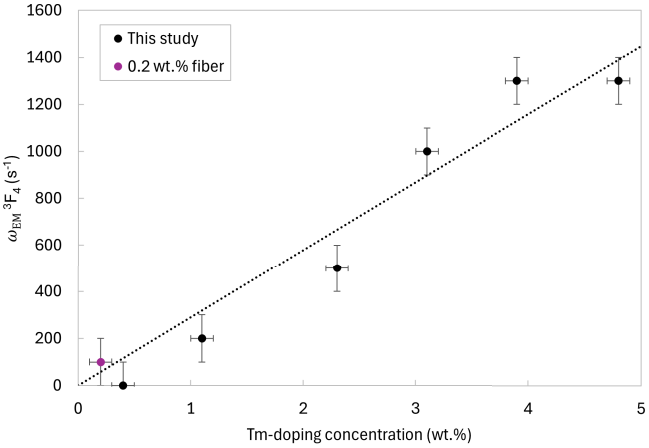

Fig. 9. The rate parameter of energy migration of the $^3F_4$ level extrapolated to a launched pump power of 0 mW, as a function of Tm^{3+}-doping concentration for the fibers in this study and the 0.2 wt.% fiber from [11].

A complete summary of the results obtained from analysis of the $^3H_4$ fluorescence decays can be found in Table 3.

Table 3. A summary of the results obtained by analysis of the $^3F_4$ fluorescence decays of the fibers in this study and the 0.2 wt.% fiber from [11]. The results of the 0.2 wt.% fiber from [11] have been adjusted to include the contribution from EM. These values of W_{ETU1+2} are valid in the limit high pump power. The values of ω_{EM}^{3F4} are valid in the limit of '0' pump power.

Fiber ID	τ_{intr}^{3F4} (μs)	τ^{3F4} (μs)	W_{ETU1+2} (10^3 s^{-1})	$k_{1120}+k_{1130}$ (10^{-23} m^3s^{-1})	ω_{EM}^{3F4} (10^3 s^{-1})
0 (from [11])	467±6	337±10	820±120	2.3-6.4	0.1±0.1
1	406±8	406±8	0	0	0.0±0.1
2	498±7	371±7	690±80	0.80±0.17	0.2±0.1
3	570±5	284±17	1770±220	0.99±0.17	0.5±0.1
4	435±5	191±10	2940±300	1.22±0.16	1.0±0.1
5	469±4	169±3	3800±120	1.25±0.07	1.3±0.1
6	468±4	142±2	4890±120	1.31±0.06	1.3±0.1

5. Discussion

When we survey reports of studies into the determination of the energy transfer parameters for Tm^{3+}-doped aluminosilicate fibers, the combined ETU rate, W_{ETU1+2}, divided by CR rate, W_{CR}, is often referenced. Our previous study [11] presents a tabular comparison of this reported ratio over a number of literature studies. One key finding from the present study is the distinct difference

Optical Materials EXPRESS

between the functional form of W_{CR} vs N_{Tm} (see Fig. 4) compared to W_{ETU1+2} vs N_{Tm} (see Fig. 7). The result is a variation in the ratio of CR rate to ETU rate over the range of Tm^{3+}-doping concentrations studied, as shown in Fig. 10. We observe that the role of ETU increases linearly relative to CR with increasing Tm^{3+} concentration with ETU reaching approximately 10% of the rate of CR as the Tm^{3+} concentration approaches 5 wt.%. This fact adds to the notion that the optimal Tm^{3+} concentration when doped into aluminosilicate glass is <5 wt.%; a fact already made above in terms of the rate of CR alone. Note that the ETU/CR rate ratio for the 0.2 wt.% fiber is high relative to the fibers measured in this study. This result suggests that for fibers with non-negligible levels of clustering, the rates for ETU for the $^3F_4$ level are more affected than CR associated with the $^3H_4$ level. These are important considerations for the design of Tm^{3+}-doped aluminosilicate fibers for laser devices.

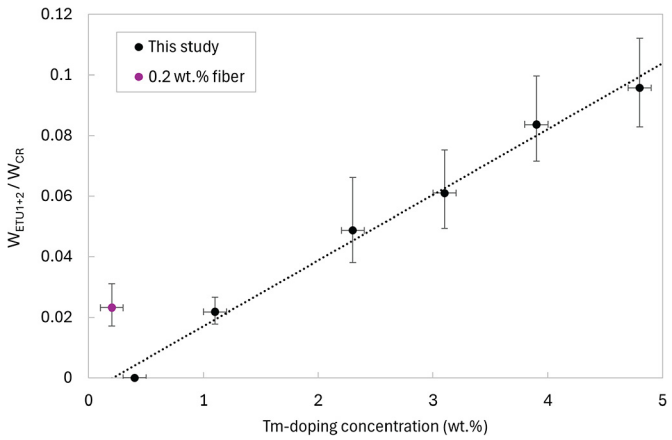

Fig. 10. The value of W_{ETU1+2} / W_{CR} as a function of Tm^{3+}-doping concentration for the fibers in this study and the 0.2 wt.% fiber from [11].

The CR rate parameter is fundamentally important to all Tm^{3+}-doped laser materials and hence there have been a number of studies investigating the variance of this parameter with Tm^{3+} concentration. Table 4 lists the functional dependence of the CR rate parameter for a variety of host materials. What is clear is the relationship for Tm^{3+}-doped aluminosilicate glass observed in this study is not consistent with other amorphous or crystalline hosts. This distinction may result from how aluminosilicate glass fiber is made compared to the other materials listed i.e., there may exist some compositional variation in aluminosilicate glass that forces a nonuniform distribution of Tm^{3+} ions and significant variation of the Tm^{3+} ion local environment. While we observe a rapid rise in the CR rate of aluminosilicate glass for concentrations <0.4 wt.%, the rate appears to stabilize for Tm^{3+} concentrations >0.4 wt.% into a much slower increase with Tm^{3+} concentration compared to other materials. A point to note from Table 4 is the slight variance observed with tellurite glass which may confirm the suggestion that some glasses present a certain complexity to energy transfer as the donor-acceptor concentration is increased.

As shown in Eq. (4), γ_{CR} is intrinsically linked to the mean intrinsic fluorescence lifetime, τ_{intr} via the ratio of Tm^{3+}-doping concentration, C, and the critical concentration, C_0, according to Foster theory [16,17]. Similarly, this can also be expressed as the ratio of average ion separation distance, R_{Tm}, to the critical ion separation distance, R_0, cubed. Figure 11 shows the values of C_0 and R_0, calculated from the values of γ_{CR} and τ_{intr} obtained during the analysis of the $^3H_4$ level decays, as a function of Tm^{3+}-doping concentration. Also shown in Fig. 11 is the actual average ion separation distance, R_{Tm} (crosses), for each Tm^{3+}-doping concentration. When converted to a critical concentration, C_0, the increase in C_0 with doping concentration is linear. The calculated

Optical Materials EXPRESS

Table 4. The relationship between CR rate parameter, W_{CR}, and Tm^{3+}-doping concentration, N_{Tm} reported in this study and a selection of other literature studies [20–25].

Reference	Host material	Relationship between W_{CR} and N_{Tm}	Notes
This work	Aluminosilicate (glass)	$\propto N_{Tm}$ for >0.4 wt.%.	The first study analyzing the CR rate parameter in aluminosilicate as a function of Tm^{3+}-doping concentration. Rapid increase in W_{CR} predicted for low Tm^{3+} concentrations (<0.4 wt.%).
Loiko and Pollnau (2016) [20]	Al_2O_3 (glass)	$\propto N_{Tm}{}^2$	This model fits the shape of fluorescence decays to population density rate equations. W_{CR} relationship has been inferred from the linear trend between k_{3011} and N_{Tm}.
Loiko et al. (2020) [21]	CaF_2 (crystal)	$\propto N_{Tm}{}^2$	Uses same approach as [20]. ETU1 and ETU2 rates also shown to increase with the same relationship as CR rate.
Gomes et al. (2012) [22]	Tellurite (glass)	$\propto N_{Tm}{}^{2.4}$	Values obtained by using a similar approach to this study. However W_{CR} is calculated with respect to τ_R, instead of τ_m.
Taher et al. (2011) [23]	Tellurite (glass)	$\propto N_{Tm}{}^2$	W_{CR} relationship has been inferred from the linear trend between k_{3011} and N_{Tm}. Analysis requires measurement of the frequency bandwidth of the emission spectra and the ratio of the strength of emission from $^3H_4$ and $^3F_4$.
Armagan et al. (1991) [24]	YAG (crystal)	$\propto N_{Tm}{}^2$	Assumption is made that the $^3H_4$ fluorescence decays in Tm:YAG represent a single exponential for this host. τ_{intr} simply found by extrapolating τ back to a Tm^{3+} concentration of '0'.
Zheng et al. (2023) [25]	Y_2O_3, Lu_2O_3, and Sc_2O_3 (crystals)	$\propto N_{Tm}{}^2$	This analysis is based on the ratio of emission intensity from $^3F_4 \rightarrow {}^3H_6$ and $^3H_4 \rightarrow {}^3F_4$.

values of R_0 rapidly increase as the Tm^{3+}-doping concentration is lowered, indicating that the *average* strength of the CR process is higher, per Tm^{3+} ion. This is also supported by the results of Fig. 4 and probably has its origins relating to the particularly high level of disorder associated with aluminosilicate glass, discussed above. The value of R_0 is asymptotic towards a constant value of around 0.9 nm at the highest doping concentrations. In addition, the difference between R_0 and R_{Tm} is becoming negligibly small at the highest Tm^{3+} concentrations. This is indicative that as the doping concentration approaches 5 wt.%, the rate of de-excitation of the $^3H_4$ level via energy transfer is approximately equal to the rate of spontaneous de-excitation through the usual radiative and NR mechanisms.

6. Summary and conclusions

We have extended the decay time segmentation and curve fitting approach to the detailed examination of the relationship between the EM, CR and ETU parameters as a function of the Tm^{3+} concentration for a range of Tm^{3+}-doped aluminosilicate glass fibers. We find that the rate of CR appears anomalously high for low Tm^{3+} concentrations, although more results are needed to confirm this finding. We show that EM plays an essential role in the energy transfer dynamics for Tm^{3+}-doped aluminosilicate glass, displaying a greater role within the CR and ETU processes as the Tm^{3+} concentration is increased. We compared our results of the CR

Optical Materials EXPRESS

rates for aluminosilicate glass with other Tm^{3+}-doped materials and found that aluminosilicate glass has distinctly different behavior when compared to other materials. We postulate that aluminosilicate glass may present a particularly high level of disorder, producing a wide variety of nearest neighbor environments that has a non-negligible impact on energy transfer.

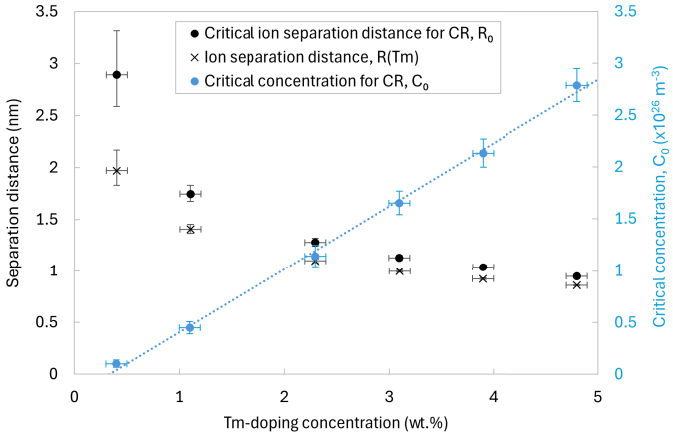

Fig. 11. Calculated values of critical ion separation distance for cross relaxation, R_0, average ion separation distance, R_{Tm}, and critical concentration for cross relaxation, C_0, as a function of Tm^{3+}-doping concentration.

Funding. Air Force Office of Scientific Research (FA2386-23-1-4115).

Acknowledgment. The authors would like to acknowledge the fiber fabrication facility of the Optoelectronics Research Centre, University of Southampton for fabrication of the fibers used in this study.

Disclosures. The authors declare no conflicts of interest.

Data availability. The data that supports the findings of this study is available from the corresponding author upon reasonable request.

References

1. S. D. Jackson and T. A. King, "Theoretical modeling of tm-doped silica fiber lasers," J. Lightwave Technol. **17**(5), 948–956 (1999).
2. S. D. Jackson, "Cross relaxation and energy transfer upconversion processes relevant to the functioning of 2 μm tm^{3+}-doped silica fibre lasers," Opt. Commun. **230**(1-3), 197–203 (2004).
3. A. Sincore, J. D. Bradford, J. Cook, *et al.*, "High average power thulium-doped silica fiber lasers: Review of systems and concepts," IEEE J. Sel. Top. Quantum Electron. **24**(3), 1–8 (2018).
4. P. varák, M. Leich, M. Kamrádek, *et al.*, "Nanoparticle doping and molten-core methods towards highly thulium-doped silica fibers for 0.79 μm-pumped 2 μm fiber lasers – a fluorescence lifetime study," J. Lumin. **275**, 120835 (2024).
5. J. Cajzl, P. Peterka, M. Kowalczyk, *et al.*, "Thulium-doped silica fibers with enhanced fluorescence lifetime and their application in ultrafast fiber lasers," Fibers **6**(3), 66 (2018).
6. J. Cajzl, P. Peterka, P. Honzátko, *et al.*, "Evaluation of energy transfer coefficients in Tm-doped fibers for fiber lasers," in *Photonics, Devices, and Systems VII*, vol. 10603 K. Fliegel and P. Páta, eds., International Society for Optics and Photonics (SPIE, 2017), p. 106030G.
7. M. Kamrádek, J. Aubrecht, P. Vařák, *et al.*, "Energy transfer coefficients in thulium-doped silica fibers," Opt. Mater. Express **11**(6), 1805–1814 (2021).
8. B. M. Anderson, J. Solomon, and A. Flores, "1.1 kW, beam-combinable thulium doped all-fiber amplifier," in *Fiber Lasers XVIII: Technology and Systems*, vol. 11665 M. N. Zervas, ed., International Society for Optics and Photonics (SPIE, 2021), p. 116650B.
9. R. Tumminelli, V. Petit, A. Carter, *et al.*, "Highly doped and highly efficient Tm doped fiber laser (Conference Presentation)," in *Fiber Lasers XV: Technology and Systems*, vol. 10512 I. Hartl and A. L. Carter, eds., International Society for Optics and Photonics (SPIE, 2018), p. 105120M.
10. S. Gausmann, B. Faugas, J. Bradford, *et al.*, "High concentration large-mode-area Tm-doped double-clad fiber for high efficiency operation," in *Fiber Lasers XX: Technology and Systems*, vol. 12400 V. R. Supradeepa, ed., International Society for Optics and Photonics (SPIE, 2023), p. 124000L.

Optical Materials EXPRESS

11. M. P. Buckthorpe and S. D. Jackson, "Revisiting energy transfer in tm-doped aluminosilicate glass fiber i: introducing a new model," Opt. Mater. Express **15**(10), 2576–2591 (2025).
12. W. Blanc, T. Sebastian, B. Dussardier, *et al.*, "Thulium environment in a silica doped optical fibre," J. Non-Cryst. Solids **354**(2-9), 435–439 (2008). Physics of Non-Crystalline Solids 11.
13. B. Faure, W. Blanc, B. Dussardier, *et al.*, "Thulium-doped silica-fiber based s-band amplifier with increased efficiency by aluminum co-doping," in *Optical Amplifiers and Their Applications/Integrated Photonics Research*, (Optica Publishing Group, 2004), p. OWC2.
14. R. Švejkar, N. Choudhury, T. G. Harris, *et al.*, "Dependence of quantum efficiency and core propagation loss on doping concentration in tm-doped silica fibers," Opt. Express **33**(23), 48807–48814 (2025).
15. A. Burshtein, "Energy transfer kinetics in disordered systems," J. Lumin. **34**(4), 167–188 (1985).
16. M. Inokuti and F. Hirayama, "Influence of energy transfer by the exchange mechanism on donor luminescence," The J. Chem. Phys. **43**(6), 1978–1989 (1965).
17. T. Forster, "10th spiers memorial lecture. transfer mechanisms of electronic excitation," Discuss. Faraday Soc. **27**(0), 7–17 (1959).
18. O. Humbach, H. Fabian, U. Grzesik, *et al.*, "Analysis of oh absorption bands in synthetic silica," J. Non-Cryst. Solids **203**, 19–26 (1996).
19. P. C. Shardlow, D. Jain, R. Parker, *et al.*, "Optimising tm-doped silica fibres for high lasing efficiency," in *2015 European Conference on Lasers and Electro-Optics - European Quantum Electronics Conference*, (Optica Publishing Group, 2015), pp. CJ–14–3.
20. P. Loiko and M. Pollnau, "Stochastic model of energy-transfer processes among rare-earth ions. example of al^2o^3:tm^{3+}," J. Phys. Chem. C **120**(46), 26480–26489 (2016).
21. P. Loiko, A. Braud, L. Guillemot, *et al.*, "Cross-relaxation and ion clustering in tm^{3+}: Caf2 crystals," in *Fiber Lasers and Glass Photonics: Materials through Applications II*, vol. 11357 (SPIE, 2020), pp. 120–125.
22. L. Gomes, J. Lousteau, D. Milanese, *et al.*, "Energy transfer and energy level decay processes in tm^{3+}-doped tellurite glass," J. Appl. Phys. **111**(6), 063105 (2012).
23. M. Taher, H. Gebavi, S. Taccheo, *et al.*, "Novel approach towards cross-relaxation energy transfer calculation applied on highly thulium doped tellurite glasses," Opt. Express **19**(27), 26269–26274 (2011).
24. G. Armagan, A. Buoncristiani, and B. Di Bartolo, "Excited state dynamics of thulium ions in yttrium aluminum garnets," Opt. Mater. **1**(1), 11–20 (1992).
25. L. Zheng, H. Wu, L. Zhang, *et al.*, "Determination of cross-relaxation efficiency based on spectroscopy in thulium-doped rare-earth sesquioxides," Ceram. Int. **49**(7), 11060–11066 (2023).